HHS Public Access

Author manuscript

Angew Chem Int Ed Engl. Author manuscript; available in PMC 2021 February 24.

Published in final edited form as:

Angew Chem Int Ed Engl. 2020 February 24; 59(9): 3711–3717. doi:10.1002/anie.201914434.

Self-amplified Photodynamic Therapy through $^1O_2$-mediated In Situ Internalization of Photosensitizers from a Ppa-bearing Block Copolymer

Zhiyong Liu[+,a], **Tianye Cao**[+,b,c], **Yudong Xue**[a], **Mengting Li**[b], **Mengsi Wu**[a], **Jonathan W. Engle**[b], **Qianjun He**[c], **Weibo Cai**[b], **Minbo Lan**[a], **Weian Zhang**[a]

[a]Shanghai Key Laboratory of Functional Materials Chemistry, East China University of Science and Technology, 130 Meilong Road, Shanghai 200237, China

[b]Departments of Radiology and Medical Physics, University of Wisconsin-Madison, Madison, WI, 53705, USA

[c]Guangdong Provincial Key Laboratory of Biomedical Measurements and Ultrasound Imaging, National - Regional Key Technology Engineering Laboratory for Medical Ultrasound, School of Biomedical Engineering, Health Science Center, Shenzhen University, No. 1066 Xueyuan Road, Nanshan District, Shenzhen, 518060 Guangdong, China

Abstract

Nanocarriers are employed to deliver photosensitizers for photodynamic therapy (PDT) through the enhanced penetration and retention effect, but disadvantages including the premature leakage and non-selective release of photosensitizers are still existing. Herein, we developed a $^1O_2$-responsive block copolymer (POEGMA-*b*-P(MAA-*co*-VSPpaMA) to enhance PDT via precisely controllable release of photosensitizers. Once nanoparticles formed by the block copolymer were accumulated in tumor and taken up by cancer cells, pyropheophorbide-a (Ppa) could be controllably released via the trigger of singlet oxygen ($^1O_2$) generated by a short duration light irradiation, thus enhancing the photosensitization, which was demonstrated by confocal laser scanning microscopy and in vivo fluorescence imaging. Consequently, benefiting from the $^1O_2$-responsiveness of POEGMA-*b*-P(MAA-*co*-VSPpaMA) block copolymer, a self-amplified photodynamic therapy could be well realized by regulating the release of Ppa with NIR illumination for enhancing the sensitization of Ppa, which may provide a new insight into the design of precise PDT.

Graphical Abstract

wazhang@ecust.edu.cn.

[+]These authors contributed equally.

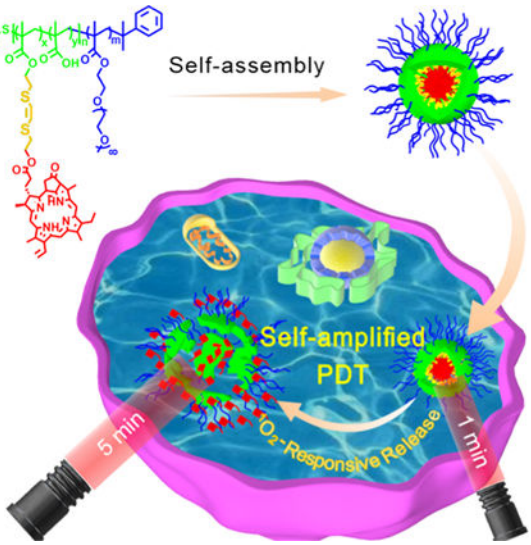

We developed a self-amplified PDT system by $^1O_2$-responsive Ppa-bearing block copolymer based on the breakage of vinyldithioether by the generated $^1O_2$ under laser irradiation followed by the in situ release of Ppa from the VSP nanoparticles, thereby enhancing the photosensitization of Ppa. The PDT efficiency was significantly improved by the $^1O_2$-mediated internalization and amplification effect of Ppa.

Keywords

controllable release; $^1O_2$-responsive; self-amplified; photodynamic therapy; block copolymer

Introduction

Photodynamic therapy (PDT) involves photosensitizers (PSs) and an appropriate wavelength light source to convert oxygen to reactive oxygen species (ROS), especially singlet oxygen ($^1O_2$), which can induce irreversible damage of cancer tissue.[1] Though PDT has been a promising option for cancer treatment owing to its non-invasiveness, the photosensitizer as an important role of PDT still faces many barriers such as poor water-solubility, non-selectivity and poor biocompatibility for the restriction of PDT in clinical practice.[2] To overcome these limitations, nanocarriers[2] such as polymer nanoparticles,[3] liposomes,[4] dendrimers[5] and inorganic nanoparticles[6] or other kind nanoparticles[7] have been developed for the delivery of these hydrophobic drugs to prolong blood circulation and enhance the accumulation of drugs in tumor tissues by enhanced permeation and retention (EPR) effect.[8] The drug delivery efficiency of hydrophobic drugs such as photosensitizers was obviously enhanced by the nanocarriers, but many limitations still exist such as the premature leakage and non-selective release of photosensitizers.[2]

Recently, stimuli-responsive drug delivery systems have drawn increasing attention, since they can effectively expose the hydrophobic drugs to tumor sites.[9] Considering the specific endogenous microenvironmental of tumors, such as lower interstitial pH,[10] higher glutathione concentration[11] and ROS levels[12] or elevated level of certain enzymes,[13]

many internal stimuli-responsive polymeric prodrugs as a typical kind of nanocarriers have been developed. Although these polymeric prodrugs can avert drug leakage during circulation in vivo, the release of drugs in tumor is uncontrollable due to the heterogeneity of tumor cells. To command the release of PSs at the tumor sites, exogenous stimuli-responsive PS delivery systems also have been constructed, such as thermo-[14] and light-[15] sensitive nanoparticulate systems. Owing to the non-invasive nature and the potential of precisely spatiotemporal control, a range of photo-responsive systems have been engineered by using exogenous light irradiation.[16] However, most of photochromic moieties such as azobenzene[17] suffer from various drawbacks such as low penetration depth and skin injury because of the harmful UV light response. Although UCNPs[18] have been proposed to convert near infrared light to overcome the limitation, the low energy conversion efficiency and expensive cost still exist in treatments. Singlet oxygen ($^1O_2$) is extremely reactive and can react with electron rich olefins such as vinyldithioether to form fragment for liberating photosensitizers, which could enhance the photodynamic therapy or activate fluorescence emission.[19] Moreover, the sulfur-containing compounds can undergo a hydrophobic to hydrophilic transition under ROS, which may facilitate the release of photosensitizers conjugated to the $^1O_2$-responsive linker.[20] In consideration of $^1O_2$ generated by photosensitizers in photodynamic therapy, it would be smart to develop a light-triggered $^1O_2$-responsive system for in situ release of photosensitizers to enhance photodynamic effect.

Herein, we developed a Ppa-containing polymer based on POEGMA-*b*-P(MAA-*co*-VSPpaMA) block copolymer by a $^1O_2$-responsive linker for controlled release of photosensitizers in situ to enhance photodynamic therapy (Scheme 1). POEGMA-*b*-PMAA block copolymer was first prepared by reversible addition-fragmentation chain transfer (RAFT) polymerization, and then vinyldithioether as a $^1O_2$-cleavable linker was used to conjugate photosensitizer Ppa and PMAA as the hydrophobic segment to form amphiphilic block copolymer POEGMA-*b*-P(MAA-*co*-VSPpaMA). Therefore, the following advantageous characteristics would be realized: i) conjugated Ppa could be controllably released from nanoparticles using the generated $^1O_2$ during laser treatment, thereby enhancing the therapeutic photoactivity; ii) directly utilizing near-infrared irradiation, high-efficiency and greater penetration depth could be carried out; iii) Ppa was conjugated to the polymer chain via a $^1O_2$-cleavable linker, leading to a high drug loading efficiency and controllable release ability; iv) the nanoparticles were formed from amphiphilic copolymers, endowing Ppa-based polymeric prodrugs with a high biocompatibility. v) Ppa possesses inherent fluorescence and can coordinate with metal ions, endowing Ppa-based polymeric prodrugs with the ability of in vivo fluorescence imaging and chelator-free labeling of ^{64}Cu for positron emission tomography (PET) imaging.

Results and Discussion

Synthesis and self-assembly of POEGMA-*b*-P(MAA-*co*-VSPpaMA) block copolymer.

The synthesis of POEGMA-*b*-P(MAA-*co*-VSPpaMA) block copolymer is illustrated in Scheme S1 and S2. The biocompatible POEGMA[21] was first prepared by RAFT polymerization of OEGMA, and then *t*BMA was selected as the second monomer to prepare

POEGMA-*b*-P*t*BMA block copolymer via utilizing POEGMA as the macro-RAFT agent. GPC (Figure S1) and ^{1}H NMR (Figure S2–S4) were used to determine the successful synthesis of POEGMA and POEGMA-*b*-P*t*BMA. Finally, POEGMA-*b*-PMAA were obtained by removing *tert*-butyl ester groups of POEGMA-*b*-P*t*BMA (Figure S5 and S6). Ppa was functionalized by $^1O_2$-responsive vinyldithioether[22] to produce VSPpa-OH via Steglich esterification, and then VSPpa-OH was further conjugated to the POEGMA-*b*-PMAA block copolymer to obtain the $^1O_2$-responsive POEGMA-*b*-P(MAA-*co*-VSPpaMA) block copolymer (denoted as '**VSP**'). The grafting ratio of Ppa was about 60%, which is determined through fluorescence spectroscopy and ^{1}H NMR spectrum. The POEGMA-*b*-P(MAA-*co*-OCPpaMA), POEGMA-*b*-P(MAA-*co*-VSPpaMA)2 and POEGMA-*b*-P(MAA-*co*-DMEPpaMA) block copolymers (denoted as **OCP**, **VSP2** and **DMEP**, respectively) as the control samples were also synthesized by a similar approach described above (Scheme S3 and S4), and the detailed characterizations are given in Figure S7–S14.

The assembled nanoparticles were prepared by dropwise adding block copolymer tetrahydrofuran (THF) solution into deionized water under rapid stirring, and then dialyzing the mixture against the ultrapure water to remove THF. The critical micelle concentration (CMC) in the ultrapure water could be obtained by fluorescence spectra using pyrene as the fluorescent probe, and the ratio changes of pyrene at 383 and 372 nm (I_{383}/I_{372}) were recorded with a fluorescence spectrophotometer.[23] As shown in Figure S15, the CMC value of **VSP** and **OCP** was 2.36×10^{-3} mg/mL and 2.93×10^{-3} mg/mL, respectively.

$^1O_2$-responsive degradation of VSP nanoparticles.

TEM was used to characterize the assembled morphologies. As shown in Figure 1a and S16, spherical nanoparticles with 130 nm (**VSP** nanoparticles) and 160 nm (**OCP** nanoparticles) have been obtained. Additionally, the irregular assembled aggregates with broad size distribution were shown in Figure 1b, which is resulted from the broken nanoparticles. Dynamic lighting scatter (DLS) was also utilized to determine the size distribution of these nanoparticles. The hydrodynamic diameter of **VSP** nanoparticles (Figure 1c) was 147.31 nm with PDI = 0.126 and that of **OCP** nanoparticles (Figure S17) was 170.57 nm with PDI = 0.123. Zeta potentials of VSP and OCP nanoparticles were about −45.3 mV and −40.5 mV (Figure S18), respectively, indicating the excellent colloidal stability of nanoparticles. After a short duration irradiation at 660 nm, **VSP** nanoparticles were destroyed, but there was almost no change for **OCP** nanoparticles (Figure 1d and S19). This result could be attributed to the $^1O_2$-mediated cleavage of vinyldithioether linker.[3d,22] The size of DLS is bigger than that measured by TEM, which can be attributed to the fact that the hydrodynamic radii are Z-averages and the POEGMA chains are extended in the solution. UV absorption and fluorescence emission spectra were also measured before and after light irradiation. Figure 1e showed a clear blue shift of the absorption peak and the absorbance at 660 nm increased, whereas that at 700 nm decreased after irradiation. These results indicate the aggregated Ppa can be released from **VSP** nanoparticles after irradiation. In addition, the fluorescence emission intensity of **VSP** nanoparticles (Figure 1f) was much higher after irradiation, which demonstrates a potential capability of response-triggered fluorescence imaging and the existence of dissociated Ppa. Moreover, almost no Ppa was released from both **OCP** and **VSP** nanoparticles without single oxygen (Figure 2a). However, an evident Ppa release can

be observed from **VSP** nanoparticles upon the production of $^1O_2$ under NIR light irradiation, and around 40% of conjugated Ppa was released from **VSP** nanoparticles in 4 h after NIR light irradiation. To give an insight into the exciting result, the oxidation products were also detected. As shown in Figure S20 and S21, mercapto group can be successfully oxidized, even sulfonic acid group, thus improving the hydrophility of Ppa. The release curves of **P@Ppa** and **P@VPpa** nanoparticles further verified the promoting release effect of ROS oxidation of VSPpa-OH (Figure 22).

$^1O_2$ production of nanoparticles.

1, 3-diphenylisobenzofuran (DPBF) was used as a $^1O_2$ indicator.[24] As shown in Figure 2b, **VSP** nanoparticles without pretreatment of light irradiation showed no obvious difference in comparison with **OCP** nanoparticles, but when **VSP** nanoparticles was pretreated with light irradiation, a rapid decrease of the absorbance of DPBF was observed, meaning the more $^1O_2$ generated by irradiation. This is attributed to the $^1O_2$-responsiveness of **VSP** nanoparticles, which could enhance $^1O_2$ generation efficiency by releasing the photosensitizers from **VSP** nanoparticles treated with preillumination.

Intracellular uptake, release and photoactivity.

To demonstrate the intracellular delivery capability of the nanoparticles, cellular uptake and intracellular Ppa release behaviour of nanoparticles were evaluated using confocal laser scanning microscopy (CLSM). As shown in Figure 2c, the fluorescence intensities of **VSP** and **OCP** nanoparticles were all lower than that of free Ppa without light irradiation with the same porphyrin concentration of 5 μg/mL, indicating that the Ppa in nanoparticles was in aggregating state. After irradiation with 660 nm laser for 1 min, the fluorescence intensity of **VSP** nanoparticles increased significantly, while **OCP** nanoparticles and free Ppa were almost unchanged, suggesting that Ppa could be effectively released from **VSP** nanoparticles. The release of Ppa from **VSP** nanoparticles was further proved by the changes of curves for fluorescence intensity recorded via flow cytometry (Figure S23 and S24). Compared to the control, the curves of nanoparticles shifted to right with or without irradiation, demonstrating nanoparticles were efficiently taken up by tumor cells. Besides, exposed beforehand to 660 nm laser for 1 min, the fluorescence intensity of **VSP** nanoparticles changed obviously while that of **OCP** nanoparticles had no change, which are in agreement with the results of CLSM.

Intracellular ROS generation was also determined to evaluate the photoactivity of **VSP** nanoparticles by using DCFH-DA as a ROS indicator.[25] Upon irradiation with 660 nm laser, green fluorescence intensity of DCF increased with the extension of interval and became constant at 4 h after the pretreatment (Figure S25a). These could be attributed to the time-dependent internalization of Ppa from nanoparticles. The high fluorescence intensity confirmed significant ROS generation in tumor cells, thus 4 h interval after pretreatment would be an optimized program to enhance the photodynamic effect. While **OCP** nanoparticles showed no obvious difference after treated by 6 min or 1+5 min irradiation with the same interval (Figure S25b).

Cytotoxicity of VSP nanoparticles.

MTT assay was used to evaluate the in vitro cytotoxicity.[26] As proved in Figure 3a, no significant cytotoxicity was observed with **VSP** and **OCP** nanoparticles without light treatment, while free Ppa displayed slight cytotoxicity with the porphyrin concentration increased. These results could be attributed to the good biocompatibility of nanoparticles. In addition, with the 6 min light treatment in once time, the cell viability displayed slight reduction contrast to the dark cytotoxicity (Figure 3b). However, when treating the cells with a 4 h interval between the first 1 min irradiation and subsequent 5 min illumination, the cell viability treated with nanoparticles showed more prominent decrease than that of treatment with 6 min light illumination in one time. Meanwhile, there was no distinctive change of phototoxicity treated with free Ppa between 1+5 min and 6 min illumination (Figure 3c and 3d). Moreover, **VSP** nanoparticles exhibited more efficient therapeutic effects than **OCP** nanoparticles, which is attributed to the $^1O_2$-responsive release of porphyrin from **VSP** nanoparticles. This confirms the self-amplified photodynamic effect of **VSP** nanoparticles, and is also in agreement with above flow cytometry and CLSM results. Additionally, the cytotoxicity assay of **P@Ppa**, **P@VPpa**, **VSP2** and **DMEP** nanoparticles were also performed to further validate the promising potential as shown in Figure S26–S30. Compared with **P@Ppa** and **DMEP** nanoparticles, sulfur-containing **P@VPpa** and **VSP2** nanoparticles both revealed a more significant inhibition effect against tumor cells. These results might be ascribed to the oxidation of sulfur, which improved the hydrophility of photosensitizers.

In vivo imaging and biodistribution.

200 μL of **VSP** or **OCP** nanoparticles (1 mg/mL of Ppa) were injected into tumor bearing mice through the tail vein for in vivo fluorescence imaging. The accumulation of nanoparticles and photosensitizers release of nanoparticles in tumor site were real-time monitored by recording the fluorescence signal intensity. Owing to the EPR effect, Figure 4a demonstrated that nanoparticles were gradually accumulated in tumor site over time. After 1 min light stimuli at 24 h post-injection (p.i.), the fluorescence signal intensity of **VSP** group dramatically increased compared to that of **OCP** group, revealing the successful release of Ppa from **VSP** nanoparticles. In addition, the fluorescence signal intensity of **VSP** group decreased significantly compared with that **OCP** group at 72 h, indicating the released Ppa could be cleared rapidly.

PET imaging is a non-invasive imaging technique with unlimited signal penetration and excellent quantitative capability.[27] Among all the positron emitter radionuclides employed in PET, ^{64}Cu-labeled radiopharmaceuticals have drawn much attention due to the low positron energy and the longer half-life.[28] Thanking to the chelating nature of the porphyrin Ppa, the radionuclide ^{64}Cu (life of 12.7 h and β^+ 17.8 %) could be chelator-free labeled with VSP nanoparticles for PET imaging to investigate circulation and biodistribution.[29] The radiolabeling step was completed by mixing $^{64}CuCl_2$ (37–74MBq) with **OCP** or **VSP** nanoparticles in sodium acetate buffer (0.1 m, pH 7), by simple shaking for 120 min at 70 °C. As shown as Figure S31, we found that $^{64}Cu^{2+}$ was gradually chelated by nanoparticles with ~80% labeling yields. To investigate the tumor uptake behavior, B16F10 tumor-bearing mice (n = 3) were injected with ^{64}Cu-**OCP** and ^{64}Cu-**VSP**

nanoparticles, and the representative maximum intensity projections (MIP) are shown in Figure 4b. We found that both of ^{64}Cu-**OCP** and ^{64}Cu-**VSP** nanoparticles rapidly accumulated in tumor within 0.5 h p.i.. The tumor-targeting efficiencies of ^{64}Cu-**OCP** and ^{64}Cu-**VSP** nanoparticles were determined to be 4.7–4.1 %ID/g and 3–2.5 %ID/g from 0.5–36 h p.i., respectively (Figure S32), indicating both of them have the potential for PDT. We observed ^{64}Cu-**OCP** and ^{64}Cu-**VSP** nanoparticles accumulation in tumors compared with the surrounding muscle tissue for extended periods of time. The mean tumor-to-muscle ratios of ^{64}Cu-**OCP** and ^{64}Cu-**VSP** nanoparticles were found to be 11.25, and 6.5 at 24 h p.i., respectively. (Figure 4c and 4d). Such a satisfactory result could be attributed to the effective accumulation of nanoparticles by EPR effect. In addition, ^{64}Cu-**OCP** and ^{64}Cu-**VSP** nanoparticles were higher uptake by reticulo-endothelial system (RES) such as liver and spleen. To further investigate the biodistribution of ^{64}Cu-**OCP** and ^{64}Cu-**VSP** nanoparticles, the mice were sacrificed at 36 h and the main organs (heart, liver, spleen, pancreas, lung, kidney, and intestine together with stomach) were harvested and investigated by γ-counter analysis. As shown in Figure 4e and 4f, the signal intensities in organs were agreeable with the ROI analysis of in vivo PET imaging.

In vivo self-amplified photodynamic therapy.

Taken all together, in vivo photodynamic therapy was performed to further prove the self-amplified effect. 200 μL of 4×10^6 tumor cells were injected subcutaneously into per nude mouse. When the tumor volume reached 200 mm^3, the mice were randomly divided into seven groups (control, **OCP**, **VSP**, **OCP/6** min, **VSP/6** min, **OCP/1+5** min, **VSP/1+5** min). Then 200 μL of saline or solution (1 mg/kg of Ppa) of **OCP** or **VSP** was injected into the mice via the tail vein. At 24 h p.i., mice in groups of **OCP/6** min and **VSP/6** min were irradiated with 660 nm laser for 6 min. While mice in groups of **OCP/1+5** min and **VSP/1+5** min were illuminated with a 4 h interval between twice irradiation. Relative tumor volume and body weight were recorded to evaluate the suppressive effect. As Figure 5a, 5c and 5d shown, compared with the control group, **OCP/6** min and **VSP/6** min groups showed partial tumor growth inhibition, while 1+5 min groups showed significant inhibition of tumor volume. In addition, some extent decrease of tumor volume was observed in **VSP/1+5** min group. These results suggested photodynamic toxicity could be significantly enhanced via a short duration irradiation pretreatment, especially with the release of Ppa. $^1O_2$-responsive **VSP2** and **DMEP** nanoparticles also showcased the similar results (Figure S33 and S34). Importantly, sulfur-containing **VSP2** nanoparticles exhibited more prominent tumor inhibition effect, which may result from the oxidation of sulfur. Tumor volume of mice treated by **OCP** and **VSP** nanoparticles displayed sharp growth and no obvious difference. These can be attributed to the high biocompatibility of nanoparticles. Figure 5b demonstrated that no abnormal behavior or significant weight loss was observed in any group, revealing minimal side effects of treatment. H&E staining on tissue sections was also used to evaluate treatment efficacy and biocompatibility of nanoparticles. As shown in Figure 5e, groups without laser treated showed no obvious difference, revealing nanoparticles had little dark toxicity, while necrosis was observed on groups with laser treatment. Moreover, the group treated by **VSP/1+5** min demonstrated prominent necrosis, indicating the significant destruction of tumor cells by self-amplified PDT. H&E stain

(Figure S35) of major organs also demonstrated that **VSP** nanoparticles have a high biocompatibility.

Conclusion

In this work, a $^1O_2$-responsive system (**VSP** nanoparticles) for self-amplified photodynamic effect was successfully established by the combination of Ppa with POEGMA-*b*-PMAA via vinyl dithioether as a $^1O_2$ cleavable linker. After a short duration irradiation, photosensitizers could be released from the nanoparticles to achieve the self-amplified effect. Compared to other treatment groups, the significantly reduced viability of cells was observed in the condition incubated with **VSP** nanoparticles and illuminated twice. Both in vivo imaging and phototherapeutic results revealed the intelligent internalization and prominent effectiveness of this delivery system of PSs. These results demonstrated that $^1O_2$-sensitive drug release systems would have potential applications in photodynamic therapy.

Experimental Section

Experimental details are depicted in the Supporting Information.

Supplementary Material

Refer to Web version on PubMed Central for supplementary material.

Acknowledgements

This work was financially supported by the National Natural Science Foundation of China (No. 21574039 and 21875063).

References

[1]. Dolmans DE, Fukumura D, Jain RK, Nat. Rev. Cancer 2003, 3, 380–387. [PubMed: 12724736]

[2]. Lucky SS, Soo KC, Zhang Y, Chem. Rev 2015, 115, 1990–2042. [PubMed: 25602130]

[3]. a)Han Y, Chen Z, Zhao H, Zha Z, Ke W, Wang Y, Ge Z, J. Controlled Release 2018, 284, 15–25;b)Zheng L, Zhang X, Wang Y, Liu F, Peng J, Zhao X, Yang H, Ma L, Wang B, Chang C, Wei H, Biomacromolecules 2018, 19, 3874–3882; [PubMed: 30107727] c)Seah GL, Yu JH, Yang MY, Kim WJ, Kim JH, Park K, Cho JW, Kim JS, Nam YS, J. Controlled Release 2018, 286, 240–253;d)Saravanakumar G, Lee J, Kim J, Kim WJ, Chem. Commun 2015, 51, 9995–9998.

[4]. a)Jin CS, Lovell JF, Chen J, Zheng G, ACS Nano 2013, 7, 2541–2550; [PubMed: 23394589] b)Yu B, Goel S, Ni D, Ellison PA, Siamof CM, Jiang D, Cheng L, Kang L, Yu F, Liu Z, Barnhart TE, He Q, Zhang H, Cai W, Adv. Mater 2018, 30, 1704934;c)Jia HR, Zhu YX, Xu KF, Liu X, Wu FG, J. Controlled Release 2018, 286, 103–113;d)Rahman MM, Ueda M, Hirose T, Ito Y, J. Am. Chem. Soc 2018, 140, 17956–17961; [PubMed: 30525544] e)Zhang K, Zhang Y, Meng X, Lu H, Chang H, Dong H, Zhang X, Biomaterials 2018, 185, 301–309; [PubMed: 30265899] f)Lovell JF, Jin CS, Huynh E, Jin H, Kim C, Rubinstein JL, Chan WC, Cao W, Wang LV, Zheng G, Nat. Mater 2011, 10, 324–332. [PubMed: 21423187]

[5]. a)Barnard A, Posocco P, Pricl S, Calderon M, Haag R, Hwang ME, Shum VW, Pack DW, Smith DK, J. Am. Chem. Soc 2011, 133, 20288–20300; [PubMed: 22040056] b)Lin TY, Li Y, Liu Q, Chen JL, Zhang H, Lac D, Zhang H, Ferrara KW, Wachsmann-Hogiu S, Li T, Airhart S, deVere White R, Lam KS, Pan CX, Biomaterials 2016, 104, 339–351; [PubMed: 27479049] c)Zhou Y, Huang W, Liu J, Zhu X, Yan D, Adv. Mater 2010, 22, 4567–4590; [PubMed: 20853374] d)Li Y, Lin TY, Luo Y, Liu Q, Xiao W, Guo W, Lac D, Zhang H, Feng C, Wachsmann-Hogiu S, Walton

JH, Cherry SR, Rowland DJ, Kukis D, Pan C, Lam KS, Nat. Commun 2014, 5, 4712. [PubMed: 25158161]

[6]. Yao C, Wang P, Li X, Hu X, Hou J, Wang L, Zhang F, Adv. Mater 2016, 28, 9341–9348. [PubMed: 27578301]

[7]. a)Lan G, Ni K, Xu Z, Veroneau SS, Song Y, Lin W, J. Am. Chem. Soc 2018, 140, 5670–5673; [PubMed: 29665677] b)Chen D, Zhang G, Li R, Guan M, Wang X, Zou T, Zhang Y, Wang C, Shu C, Hong H, Wan LJ, J. Am. Chem. Soc 2018, 140, 7373–7376; [PubMed: 29799737] c)Pan X, Bai L, Wang H, Wu Q, Wang H, Liu S, Xu B, Shi X, Liu H, Adv. Mater 2018, 30, 1800180;d)Liu WL, Liu T, Zou MZ, Yu WY, Li CX, He ZY, Zhang MK, Liu MD, Li ZH, Feng J, Zhang XZ, Adv. Mater 2018, 30, 1802006;e)Zhang K, Meng XD, Cao Y, Yang Z, Dong HF, Zhang YD, Lu HT, Shi ZJ, Zhang XJ, Adv. Funct. Mater 2018, 28, 1804634;

[8]. a)Peer D, Karp JM, Hong S, Farokhzad OC, Margalit R, Langer R, Nat. Nanotechnol 2007, 2, 751–760; [PubMed: 18654426] b)Davis ME, Chen ZG, Shin DM, Nat. Rev. Drug. Discov 2008, 7, 771–782. [PubMed: 18758474]

[9]. Mura S, Nicolas J, Couvreur P, Nat. Mater 2013, 12, 991–1003. [PubMed: 24150417]

[10]. a)Gao D, Lo PC, J. Controlled Release 2018, 282, 46–61;b)Zeng XW, Liu G, Tao W, Ma Y, Zhang XD, He F, Pan JM, Mei L, Pan GQ, Adv. Funct. Mater 2017, 27, 1605985;c)Li HJ, Du JZ, Liu J, Du XJ, Shen S, Zhu YH, Wang X, Ye X, Nie S, Wang J, ACS Nano 2016, 10, 6753–6761; [PubMed: 27244096] d)Du JZ, Du XJ, Mao CQ, Wang J, J. Am. Chem. Soc 2011, 133, 17560–17563. [PubMed: 21985458]

[11]. a)Zhou ZX, Shen YQ, Tang JB, Fan MH, Van Kirk EA, Murdoch WJ, Radosz M, Adv. Funct. Mater 2009, 19, 3580–3589;b)Yu G, Zhao X, Zhou J, Mao Z, Huang X, Wang Z, Hua B, Liu Y, Zhang F, He Z, Jacobson O, Gao C, Wang W, Yu C, Zhu X, Huang F, Chen X, J. Am. Chem. Soc 2018, 140, 8005–8019; [PubMed: 29874067] c)Xia J, Zhang L, Qian M, Bao Y, Wang J, Li Y, J. Colloid Interface Sci 2017, 498, 170–181. [PubMed: 28324723]

[12]. a)Xu X, Saw PE, Tao W, Li Y, Ji X, Bhasin S, Liu Y, Ayyash D, Rasmussen J, Huo M, Shi J, Farokhzad OC, Adv. Mater 2017, 29, 1700141;b)Daum S, Reshetnikov MSV, Sisa M, Dumych T, Lootsik MD, Bilyy R, Bila E, Janko C, Alexiou C, Herrmann M, Sellner L, Mokhir A, Angew. Chem. Int. Ed 2017, 56, 15545–15549;

[13]. a)Lee SJ, Koo H, Lee DE, Min S, Lee S, Chen X, Choi Y, Leary JF, Park K, Jeong SY, Kwon IC, Kim K, Choi K, Biomaterials 2011, 32, 4021–4029; [PubMed: 21376388] b)Zhang J, Mu YL, Ma ZY, Han K, Han HY, Biomaterials 2018, 182, 269–278; [PubMed: 30142526] c)Thomas AP, Palanikumar L, Jeena MT, Kim K, Ryu JH, Chem. Sci 2017, 8, 8351–8356. [PubMed: 29619181]

[14]. a)Park W, Park SJ, Cho S, Shin H, Jung YS, Lee B, Na K, Kim DH, J. Am. Chem. Soc 2016, 138, 10734–10737; [PubMed: 27535204] b)Liu G, Zhang S, Shi Y, Huang X, Tang Y, Chen P, Si W, Huang W, Dong X, Adv. Funct. Mater 2018, 28, 1804317.

[15]. a)Park W, Bae BC, Na K, Biomaterials 2016, 77, 227–234; [PubMed: 26606448] b)Zhou Y, Ye H, Chen Y, Zhu R, Yin L, Biomacromolecules 2018, 19, 1840–1857; [PubMed: 29701952] c)Ji C, Gao Q, Dong X, Yin W, Gu Z, Gan Z, Zhao Y, Yin M, Angew. Chem. Int. Ed 2018, 57, 11384–11388;d)Dai Y, Xiao H, Liu J, Yuan Q, Ma P, Yang D, Li C, Cheng Z, Hou Z, Yang P, Lin J, J. Am. Chem. Soc 2013, 135, 18920–18929; [PubMed: 24279316]

[16]. Karimi M, Sahandi Zangabad P, Baghaee-Ravari S, Ghazadeh M, Mirshekari H, Hamblin MR, J. Am. Chem. Soc 2017, 139, 4584–4610; [PubMed: 28192672]

[17]. Xu L, Zhang W, Cai H, Liu F, Wang Y, Gao Y, Zhang W, J. Mater. Chem. B 2015, 3, 7417–7426.

[18]. Liu J, Bu W, Pan L, Shi J, Angew. Chem. Int. Ed 2013, 52, 4375–4379.

[19]. a)Adam W, Liu J-C, J. Am. Chem. Soc 1972, 94, 1206–1209;b)Atilgan A, Tanriverdi Ecik E, Guliyev R, Uyar TB, Erbas-Cakmak S, Akkaya EU, Angew. Chem. Int. Ed 2014, 53, 10678–10681.

[20]. Sun B, Luo C, Zhang X, Guo M, Sun M, Yu H, Chen Q, Yang W, Wang M, Zuo S, Chen P, Kan Q, Zhang H, Wang Y, He Z, Sun J, Nat. Commun 2019, 10, 3211. [PubMed: 31324811]

[21]. Zhang P, Jain P, Tsao C, Yuan Z, Li W, Li B, Wu K, Hung HC, Lin X, Jiang S, Angew. Chem. Int. Ed 2018, 57, 7743–7747.

[22]. Erbas-Cakmak S, Akkaya EU, Angew. Chem. Int. Ed 2013, 52, 11364–11368.

[23]. Goddard ED, Turro NJ, Kuo PL, Ananthapadmanabhan KP, Langmuir 1985, 1, 352–355. [PubMed: 21370917]

[24]. Li B, Lin L, Lin H, Wilson BC, J. Biophotonics 2016, 9, 1314–1325. [PubMed: 27136270]

[25]. Huang P, Qian X, Chen Y, Yu L, Lin H, Wang L, Zhu Y, Shi J, J. Am. Chem. Soc 2017, 139, 1275–1284. [PubMed: 28024395]

[26]. Chen M, Liang X, Gao C, Zhao R, Zhang N, Wang S, Chen W, Zhao B, Wang J, Dai Z, ACS Nano 2018, 12, 7312–7326. [PubMed: 29901986]

[27]. a)Deng X, Rong J, Wang L, Vasdev N, Zhang L, Josephson L, Liang SH, Angew. Chem. Int. Ed 2019, 58, 2580–2605;b)Cutler CS, Hennkens HM, Sisay N, Huclier-Markai S, Jurisson SS, Chem. Rev 2013, 113, 858–883. [PubMed: 23198879]

[28]. Ametamey SM, Honer M, Schubiger PA, Chem. Rev 2008, 108, 1501–1516. [PubMed: 18426240]

[29]. a)Huang H, Hernandez R, Geng J, Sun H, Song W, Chen F, Graves SA, Nickles RJ, Cheng C, Cai W, Lovell JF, Biomaterials 2016, 76, 25–32; [PubMed: 26517562] b)Yu B, Wei H, He Q, Ferreira CA, Kutyreff CJ, Ni D, Rosenkrans ZT, Cheng L, Yu F, Engle JW, Lan X, Cai W, Angew. Chem. Int. Ed 2018, 57, 218–222.

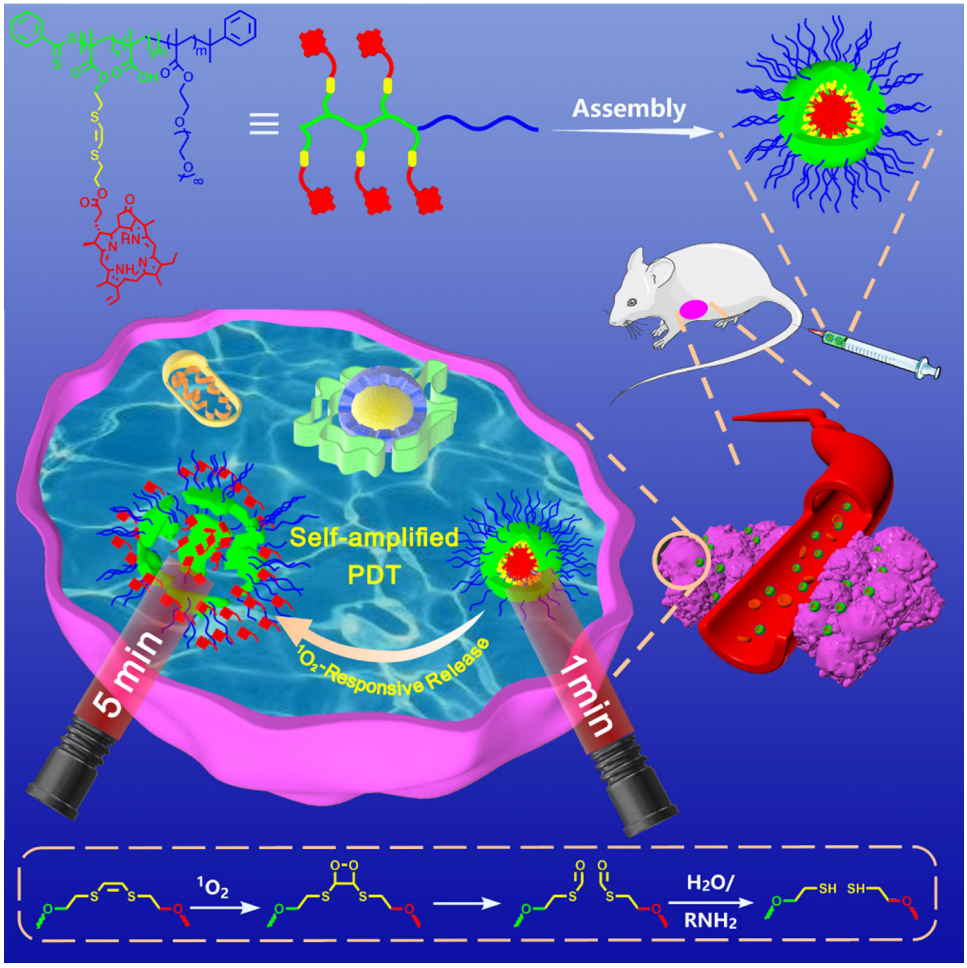

Scheme 1.

Schematic illustration of self-amplified near-infrared photodynamic therapy and the mechanism of $^1O_2$-stimuli cleavage.

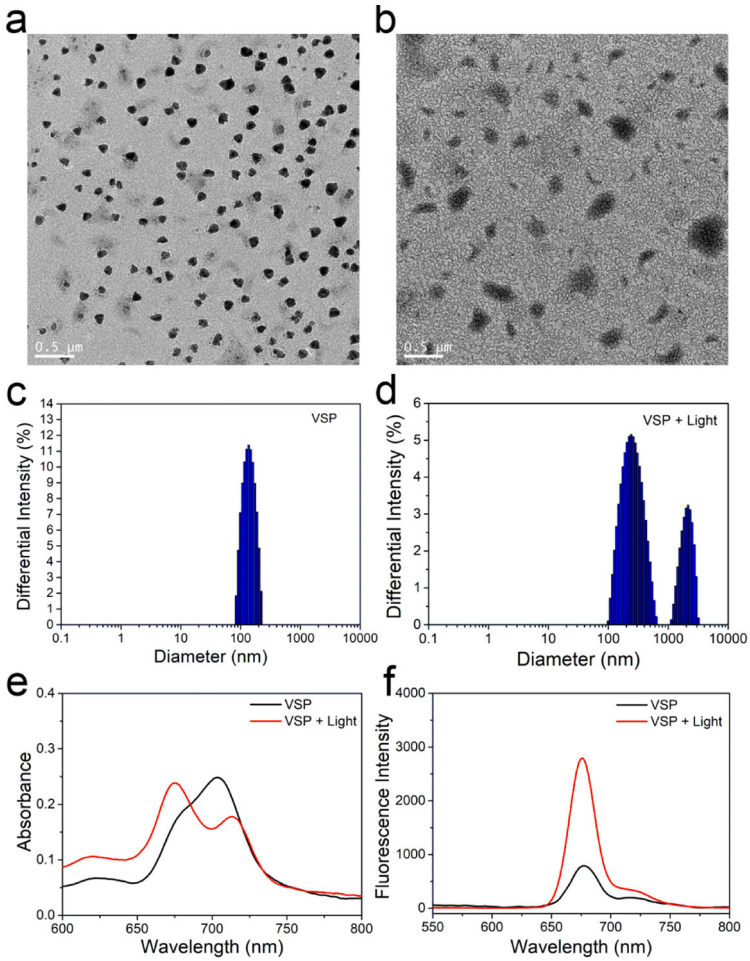

Figure 1.

Properties of **VSP** nanoparticles. TEM images of **VSP** (a) and **VSP + light** (b). Size distribution of nanoparticles determined by DLS, **VSP** (c) and **VSP + light** (d). UV spectrum (e) and fluorescence emission (f) of **VSP** before and after light irradiation.

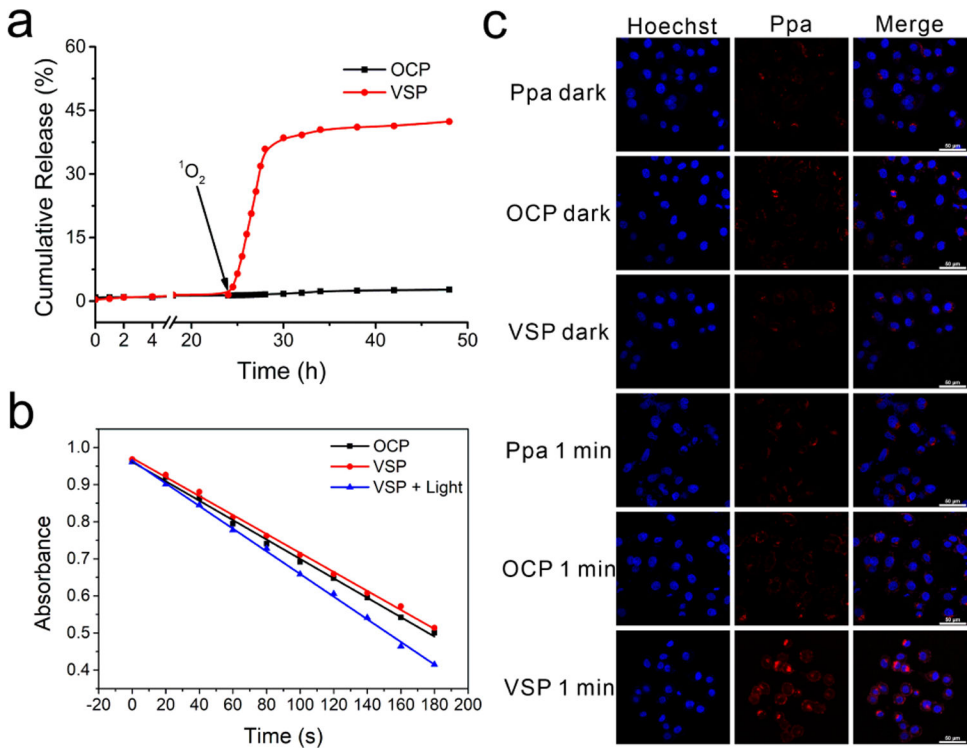

Figure 2.

(a) Ppa release curves in buffer with NIR light irradiation at 24 h for the generation of $^1O_2$. (b) $^1O_2$ generation of nanoparticles determined by DPBF as a detector. (c) Confocal laser scanning microscopy images of cellular internalization of Ppa, **VSP** and **OCP** nanoparticles treated with or without 1 min light radiation.

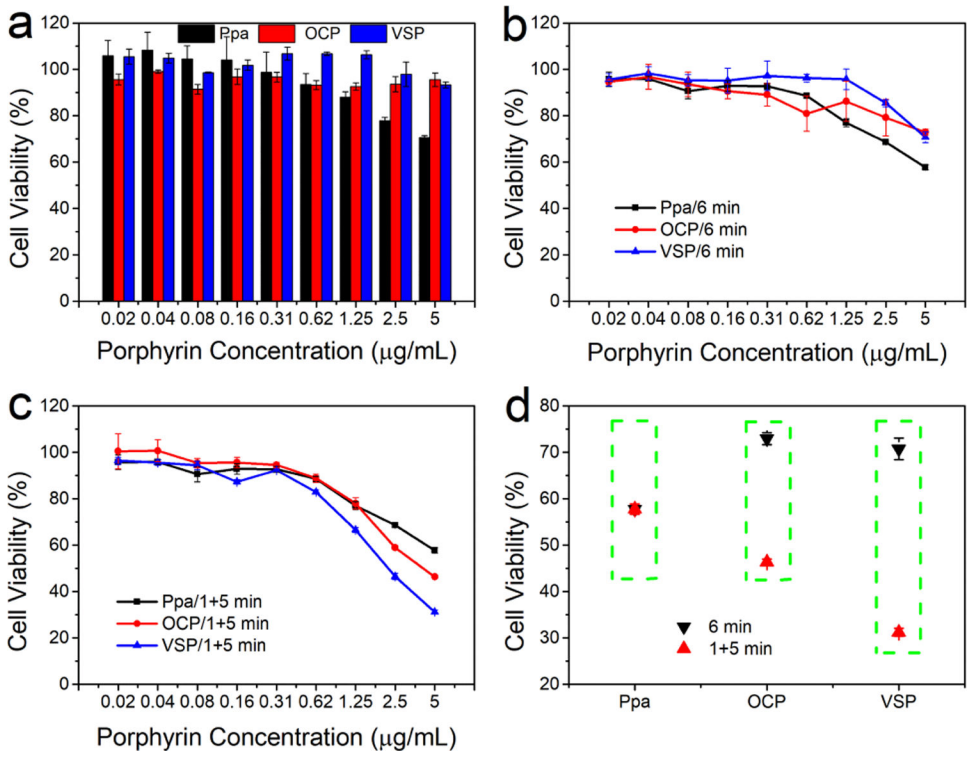

Figure 3.

In vitro cellular toxicity. (a) Without irradiation. (b) Irradiated with laser for 6 min. (c) Irradiated with laser for 1 min plus 5 min with an interval of 4 h. (d) Contrast of cell viability at 5 μg/mL under different irradiated conditions. (n = 3, mean ± s.d.).

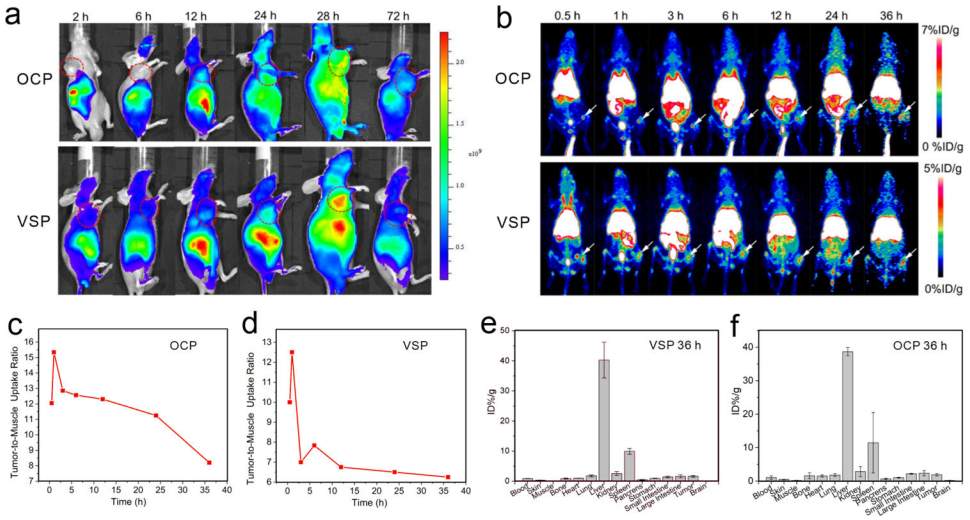

Figure 4.

(a) In vivo fluorescence imaging and (b) maximum intensity projections of PET imaging of B16F10 tumor-bearing mice after injection **OCP** and **VSP** nanoparticles with different time. Quantitative PET imaging-based accumulation kinetics of (c) ^{64}Cu-**OCP** and (d) ^{64}Cu-**VSP** nanoparticles in tumor/muscle uptake ratio. Biodistribution of (e) ^{64}Cu-**VSP** and (f) ^{64}Cu-**OCP** nanoparticles at 36 h (n = 3).

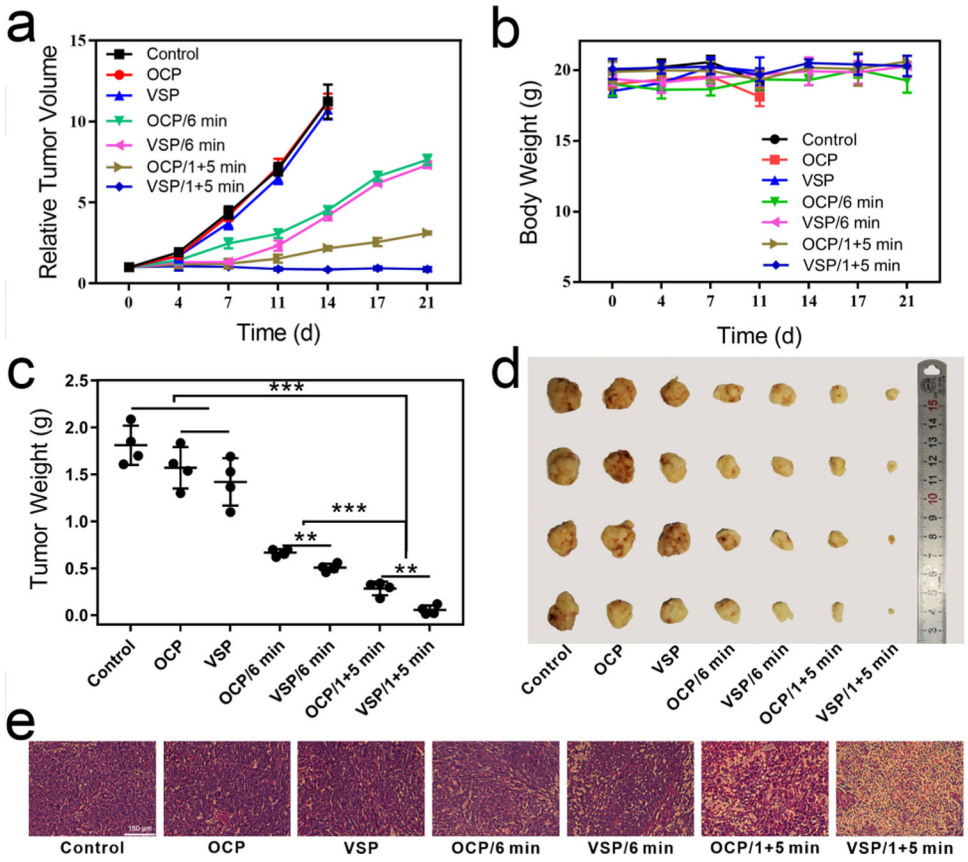

Figure 5.

In vivo anti-tumor performance with NIR irradiation. (a) Tumor inhabitation efficiency. (b) Body weight variation. (c) Tumor weight. (d) Photograph of excised tumor. (e) H&E stain of tumor tissue (400 X, scale bar = 150 μm). (n = 4, mean ± s.d., **P < 0.01, ***P < 0.001).